REVIEWS

Journal of Semiconductors
(2021) 42, 041301
doi: 10.1088/1674-4926/42/4/041301

Recent progress in integrated electro-optic frequency comb generation

Hao Sun, Mostafa Khalil, Zifei Wang, and Lawrence R. Chen†

Department of Electrical and Computer Engineering, McGill University, Montreal. QC H3A 0E9, Canada

Abstract: Optical frequency combs have emerged as an important tool enabling diverse applications from test-and-measurement, including spectroscopy, metrology, precision distance measurement, sensing, as well as optical and microwave waveform synthesis, signal processing, and communications. Several techniques exist to generate optical frequency combs, such as mode-locked lasers, Kerr micro-resonators, and electro-optic modulation. Important characteristics of optical frequency combs include the number of comb lines, their spacing, spectral shape and/or flatness, and intensity noise. While mode-locked lasers and Kerr micro-resonators can be used to obtain a large number of comb lines compared to electro-optic modulation, the latter provides increased flexibility in tuning the comb spacing. For some applications in optical communications and microwave photonics, a high degree of integration may be more desirable over a very large number of comb lines. In this paper, we review recent progress on integrated electro-optic frequency comb generators, including those based on indium phosphide, lithium niobate, and silicon photonics.

Key words: electro-optic frequency comb generation; integrated photonics; silicon photonics; integrated lithium niobate; indium phosphide

Citation: H Sun, M Khalil, Z F Wang, and L R Chen, Recent progress in integrated electro-optic frequency comb generation[J]. *J. Semicond.*, 2021, 42(4), 041301. http://doi.org/10.1088/1674-4926/42/4/041301

1. Introduction

An optical frequency comb (OFC), defined as a series of equally spaced and phase correlated discrete optical spectral lines[1], was first reported in the 1960's with the study of mode-locked lasers (MLLs)[2]. An OFC can be used as an optical frequency ruler for precision spectroscopy and was recognized with half of the 2005 Nobel Prize in Physics awarded to Hänsch and Hall[3, 4]. Over the years, the generation of OFCs has been studied intensively and their use in diverse applications have been reported, including optical frequency metrology[5], spectroscopy[6, 7], precision distance measurement (LiDAR)[8], astronomical spectrograph calibration[9, 10], optical synthesis[11], RF and microwave photonic (MWP) signal processing[12–14], and optical communications[15–17], amongst others. For example, in optical communications, OFCs can be used to generate sinc-shaped Nyquist pulses which, in turn, can be applied to Nyquist OTDM transmission. Here, the number of comb lines and comb spacing determine the duration of the sinc-shaped Nyquist pulses (more comb lines results in shorter pulses) and the repetition rate of the pulse train, respectively; the spectral flatness of the comb and mutual coherence of the comb lines determine the quality of the pulses in terms of how close they resemble the ideal sinc shape as well as the stability of the pulse train, e.g., in terms of root-mean-square (rms) timing jitter. In MWP signal processing, OFCs can be used to implement tap delay line structures for MWP filtering or for RF channelization. A large number of comb lines will enable a larger number of taps to provide increased flexibility in controlling the MWP filter response or for very broadband RF channelization. Here, an OFC with high spectral flatness is not necessary as programmable optical filters are typically used to control the amplitudes of each tap (comb line) to obtain a specific MWP filter response. Each application has its own requirements or specification on the OFC characteristics, such as the number of comb lines, spectral bandwidth, frequency or comb spacing (or free spectral range, FSR), comb power, spectral flatness, center frequency, and coherence.

These requirements have motivated different techniques for OFC generation. Approaches include MLLs[18, 19] assisted by an internal or external reference, micro-resonators with nonlinear optical effects such as four wave mixing driven by parametric oscillation[20–24] or mode locking through the formation of dissipative Kerr solitons[25, 26], chaos assisted combs in deformed microcavities[27], and electro-optic (EO) modulation[14, 17, 28–36]. MLLs can generate broad bandwidth combs, but continuous tuning of the comb spacing is very limited and specially designed laser structures are needed[19]. Pumping a micro-resonator with a single frequency laser and exploiting the nonlinear Kerr effect can generate hundreds of comb lines with extremely broad bandwidth; this approach has also been used to obtain broadband combs in the mid-IR, e.g., from 2.1 to 3.5 μm[24]. However, the formation dynamics can be complex and in order to obtain a comb with stable amplitude and phase, sophisticated control techniques are required. Moreover, for OFC generation with Kerr or chaos assisted combs, obtaining a flat spectrum as well as tunability of the comb spacing and/or the number of comb lines remains challenging[15].

On the other hand, EO modulation provides flexibility in tuning the comb features, such as comb spacing, the num-

Correspondence to: L R Chen, lawrence.chen@mcgill.ca
Received 28 OCTOBER 2020; Revised 24 JANUARY 2021.

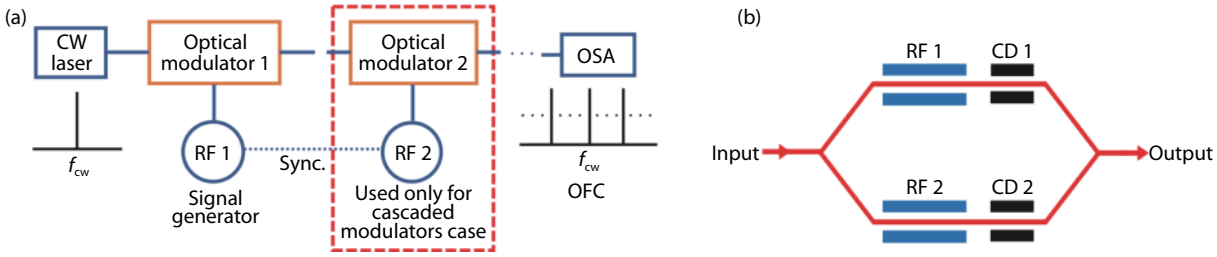

Fig. 1. (Color online) (a) Generic setup for OFC generation. (b) Schematic of a DD-MZM.

ber of comb lines, spectral flatness, etc., which can be very desirable for applications in optical communications and MWP. Here, a continuous wave signal is modulated by one or more EO modulators driven by one or more RF signal generators to create multiple sidebands. The comb spacing can be tuned by controlling the frequency (or frequencies) of the RF signal(s) while the number of comb lines can be adjusted through the number of modulators used and the corresponding driving conditions. By the appropriate selection of the modulators and careful control of the RF signals and bias voltages, a flat spectrum with high optical signal noise ratio can be obtained. Moreover, there is a growing interest for large-scale integration due to features such as efficiency, compactness, and robustness. Thanks to the advances in the development of high performance integrated EO modulators, on-chip generation of OFCs has been demonstrated in different platforms including thin film lithium niobite on insulator (LNOI)[20, 37–41], InP[42–45], silicon organic hybrid[33], and silicon-on-insulator (SOI)[17, 34, 46–53]. Various approaches have been considered, such as a single phase modulator (PM)[46], a single microring modulator (MRM)[47], a single dual drive Mach-Zehnder modulator (DD-MZM)[17], IQ or dual parallel MZMs[29] and cascaded modulators, e.g., cascaded MRMs[48–50], cascaded MZMs[51, 53], and a combination of both phase and intensity modulators (IMs)[44, 52].

In this paper, we review recent developments of integrated EO OFC generation. The purpose is not to provide a comprehensive review of the theory and different approaches, but rather to highlight some key results that have been obtained and with a specific focus on those achieved in the SOI platform. The remainder of this paper is structured as follows. We describe some basic theory of EO OFC generation in Section 2, followed by a review of the state-of-art integrated technologies in Section 3. Specifically, we describe results obtained using InP, LNOI, and SOI, including single and cascaded MRMs, single DD-MZMs, and cascaded modulators. Finally, we compare the different integrated approaches in Section 4 and conclude.

2. Electro-optic comb generation

Three main components are used for EO OFC generation: a continuous wave (CW) laser, one or more EO modulators, and RF signal generator(s), see Fig. 1(a). The output spectrum is centered at the wavelength of the CW laser and for a single EO modulator, the comb spacing is determined by the RF signal generator. Cascading two or more EO modulators leads to a greater number of comb lines and correspondingly, a larger bandwidth. The number of comb lines is dependent on the modulation depth obtained in each modulator, which in turn depends on the operating conditions such as RF power and bias voltages.

We assume a CW laser with a carrier frequency f_c and an amplitude E_i. For a single PM, the output electric field can be written as

$$E_0(t) = E_i e^{j2\pi f_c t} e^{j\phi(t)}, \tag{1}$$

where

$$\phi(t) = \frac{\pi V(t)}{V_\pi} \tag{2}$$

with $V(t)$ being the applied voltage and V_π is the half-wave voltage required to produce a π phase shift. Let us also assume that the applied voltage comprises a time-varying component, i.e., $V(t) = V_1\sin(2\pi f_m t)$. Then, the output electric field becomes $E_0(t) = E_i e^{j2\pi f_c t} e^{j\frac{\pi}{V_\pi}V_1\sin(2\pi f_m t)}$. The output signal in the frequency domain is obtained by taking the Fourier transform of $E_0(t)$ and making use of the Jacob-Anger expansion[28]:

$$\widetilde{E_o}(f) = E_i \sum_{n=-\infty}^{\infty} J_n\left(\frac{\pi}{V_\pi}V_1\right)\delta(f - nf_m - f_c), \tag{3}$$

where J_n is Bessel's function of the first kind. The factor $\delta(f - nf_m - f_c)$ represents the different comb lines in the output spectrum.

For OFC generation using a general DD-MZM [see Fig. 1(b)], we assume two RF signal generators drive the upper and lower arms of the modulator at frequencies $f_{m,1}$ and $f_{m,2}$, respectively. The output field E_0 can be written as

$$E_0(t) = \frac{E_i}{2} e^{j2\pi f_c t}[e^{j\phi_1} + e^{j\phi_2}], \tag{4}$$

where ϕ_1 and ϕ_2 are the phase shifts in the upper and lower arms of the modulator and are given by Eq. (2), i.e., $\phi_i(t) = \frac{\pi V_i(t)}{V_\pi}$ where V_i is the voltage applied across the i-th arm [$i \in \{1, 2\}$]. We let the applied voltages comprise a time-varying component, $V_i\sin(2\pi f_m t)$, and a DC bias voltage $V_{b,i}$. Eq. (4) can then be re-written as

$$E_0(t) = \frac{E_i}{2} e^{j2\pi f_c t}\left[e^{j\frac{\pi(V_1\sin(2\pi f_m t)+V_{b,1})}{V_\pi}} + e^{j\frac{\pi(V_2\sin(2\pi f_m t)+V_{b,2})}{V_\pi}}\right]. \tag{5}$$

Taking the Fourier transform of Eq. (5) gives the output signal in the frequency domain[28]:

$$\widetilde{E_o}(f) = \pi E_i \sum_{n=-\infty}^{\infty}\left[J_n\left(\frac{\pi}{V_\pi}V_1\right)e^{j\frac{\pi}{V_\pi}V_{b,1}} + J_n\left(\frac{\pi}{V_\pi}V_2\right)e^{j\frac{\pi}{V_\pi}V_{b,2}}\right]\delta(f - nf_m - f_c). \tag{6}$$

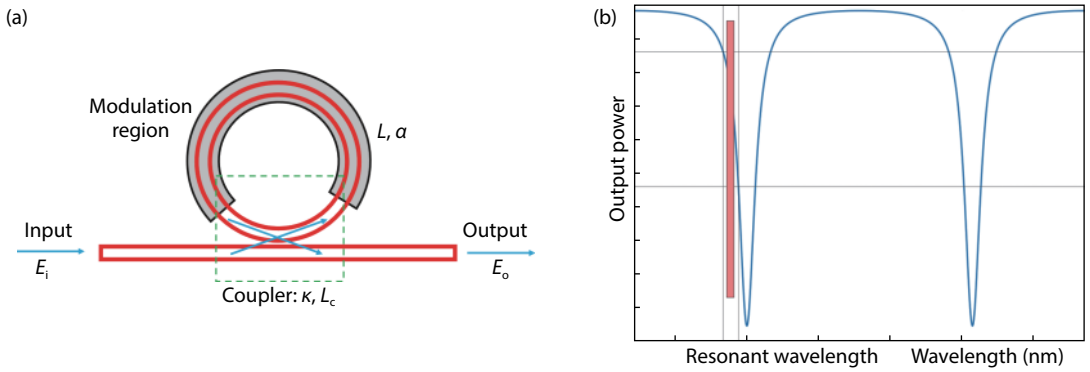

Fig. 2. (Color online) (a) Schematic of an intracavity MRM. (b) Transmission spectrum of an MRM (the input laser wavelength is shown in red for illustration).

The corresponding amplitudes of the comb lines are determined by the Bessel functions and the voltages applied to the modulators. Note that for a single-drive MZM, we can set one of the driving voltages to 0 or consider $V_2(t) = -V_1(t)$ for the case of push-pull operation.

For the case of cascading an MZM with a PM, we can express the output electric field in the time domain as[15]:

$$E_0(t) = E_i e^{j2\pi f_c t}\cos\left[\frac{\pi}{4}\alpha\sin(2\pi f_m t) - \frac{\pi}{2}\gamma\right] \times e^{j\left(\theta\frac{\pi}{4}\alpha+\frac{\pi}{2}\beta\right)\sin(2\pi f_m t)-j\theta\frac{\pi}{2}\gamma}, \tag{7}$$

where α and β are the voltages applied to the MZM and PM, respectively, and γ is the DC bias voltage of the MZM (all voltages are normalized by V_π). Proper adjustment of the voltages is required to control the number of comb lines as well as the comb flatness.

Intensity modulation in MRMs can be achieved through two means: (1) by modulating the ring waveguide (intracavity ring modulator) or (2) by modulating the coupling between the ring and the bus waveguides (coupling-modulated ring). When light propagates in the ring, it acquires a phase shift $\Delta\phi = \beta L$, where β is the corresponding propagation constant and L is the optical path length. The resonance condition must satisfy $\Delta\phi = \beta L = 2n\pi$, where n is an integer.

Fig. 2 shows a schematic of an intracavity MRM and its transmission spectrum; the red line indicates the operating wavelength of the CW input for efficient modulation. The input wavelength should lie within the most linear region of the transmission response, as in the case of MZMs. The modulation efficiency increases as the resonance of the ring is deeper, i.e., a larger extinction ratio can be obtained. However, there is a trade-off between extinction ratio and modulation bandwidth[54].

Using coupled mode theory, we can express the transfer function of the MRM as follows[46]:

$$H(f) = \frac{E_o}{E_i} = \frac{\cos(\kappa L_c) - e^{-\frac{\alpha L}{2}-j\beta L}}{1-\cos(\kappa L_c)e^{-\frac{\alpha L}{2}-j\beta L}} = \frac{v-ue^{-j\phi}}{1-uve^{-j\phi}}, \tag{8}$$

where the parameters u, v and ϕ are defined as

$$u \overset{\text{def}}{=} e^{-\frac{\alpha L}{2}}, \quad v \overset{\text{def}}{=} \cos(\kappa L_c), \quad \text{and} \quad \phi \overset{\text{def}}{=} \frac{2\pi n_{\text{eff}} L}{\lambda} = \frac{2\pi n_{\text{eff}} L}{c} f. \tag{9}$$

α is the attenuation coefficient of the ring, $L = 2\pi r$ is the perimeter of the microring with r being the radius, κ is the coupling coefficient, L_c is the coupling length, n_{eff} is the effective refractive index, and λ is the operating wavelength. The output electric field from the MRM representing the OFC is given by[20]

$$E_{\text{out}}(t) = E_{\text{in}}(t)\left[\sqrt{(1-\gamma)(1-\kappa)} - \kappa\sqrt{\frac{1-\kappa}{1-\kappa}}\frac{re^{-jm\sin(\omega_m t)}}{1-re^{-jm\sin(\omega_m t)}}\right], \tag{10}$$

where γ is the insertion loss, m is the modulation index of the modulation region (phase shifter or PM) in the MRM ($m = 0$ if the MRM does not contain a modulation region), $\omega_m = 2\pi f_m$ is the frequency from the RF signal generator, $r = \sqrt{(1-\gamma)(1-k)}\,\alpha$ is the round-trip electric field transmission, and α is the round-trip loop power transmission coefficient.

Fig. 1(a) illustrates the generic setup for OFC generation using cascaded modulators; to understand the principle of operation, we consider only two cascaded modulators. The output from a CW laser is launched into the first modulator driven by an RF signal generator at frequency f_1. For simplicity, we consider that the output comprises nominally three main tones: the carrier frequency from the laser (f_c) and the two first-order sidebands at $f_c \pm f_1$ (higher-order sidebands exist, however, the first-order sidebands can be the strongest). The second modulator, which is driven by another RF signal generator at frequency f_2, modulates these three spectral components and the final output depends on the frequency conditions used to drive both modulators. Note that the two RF signal generators must be synchronized to reduce the phase mismatch and hence, improve the quality of the output signal.

When using IMs, there are several frequency conditions that relate f_1 and f_2, with each resulting in a specific number of comb lines. We express some of these conditions as follows:

$$f_1 = 3f_2 \text{ or } f_2 = 3f_1, \qquad \Delta f = f_2, \tag{11}$$

$$f_1 = 4f_2, \qquad \Delta f = 2f_2, \tag{12}$$

$$f_1 = 2f_2, \qquad \Delta f = f_2, \tag{13}$$

where Δf is the frequency spacing between the comb lines. Fig. 3 shows the possible OFC spectra corresponding to these three conditions. For example, if we use the condition specified in Eq. (11) and drive the first MZM at $f_1 = 15$ GHz [blue

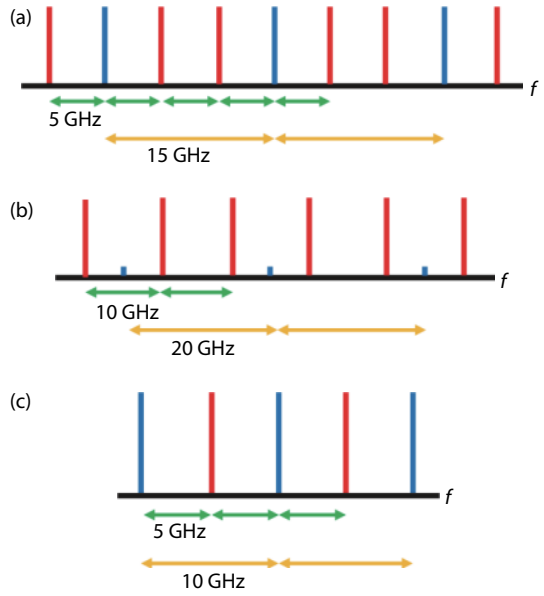

Fig. 3. (Color online) OFC generation using different driving conditions: (a) $f_1 = 3f_2$, (b) $f_1 = 4f_2$, and (c) $f_1 = 2f_2$. The blue and red lines depict the output from the first and second modulator, respectively.

lines in Fig. 3(a)] and the second MZM at f_2 = 5 GHz [red lines in Fig. 3(a)], we can obtain an output comb comprising of 9 lines with Δf = 5 GHz. On the other hand, if we use the condition specified in Eq. (12) with f_1 = 20 GHz and f_2 = 5 GHz, then some of the carriers from the second modulator will be suppressed resulting in only 6 comb lines as illustrated in Fig. 3(b). For OFC generation using cascaded MRMs and the condition specified in Eq. (13), the second MRM modulates only the middle carrier and we obtain 5 comb lines as shown in Fig. 3(c) [here f_1 = 10 GHz and f_2 = 5 GHz]. In our experiments, we have found that the conditions in Eqs. (11) and (12) work well with cascaded MZMs, while that specified in Eq. (13) is better suited for cascaded MRMs to achieve equidistant comb lines.

It is also possible to generate OFCs using a cascade of PMs and IMs, e.g., 3 PMs and an IM, or cascading a DD-MZM and a PM. Of course, cascading three or more optical modulators leads to a more complex system which requires greater control over tuning the phase shifters between the modulators and proper adjustment of the driving RF power [15, 28].

3. Integrated electro-optic comb generation

3.1. OFC generation in InP

The use of III–V materials, e.g., GaAs or InP, allows for the integration of all active components for on-chip EO OFC generation[42–45, 55–58], e.g., the laser source, modulators, and optical amplifier. In Ref. [42], Yokota and Yasaka used a traveling-wave-electrode (TWE) InP-based DD-MZM with an n–p–i–n waveguide structure and V_π ~ 2.3 V. By setting the difference in the total phase shift between the two arms of the MZM to be $\pm n\pi$ (n being an integer), they obtained 9 comb lines with a comb spacing of 12.5 GHz and a flatness < 0.8 dB.

In Ref. [43], Slavík *et al.* realized a more compact OFC generator that comprised an integrated C-band tunable laser with a dual-electrode MZM in a single package. The output optical power of the tunable laser was 13 dBm while the total loss of the push-pull modulator was ~ 6 dB (including

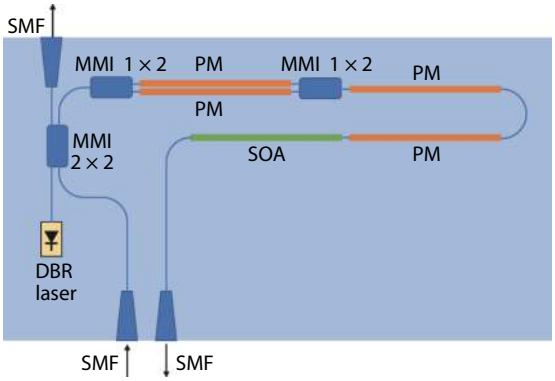

Fig. 4. (Color online) Schematic of the InP-based OFC generator in Refs. [44, 45]. SMF: single mode fiber; MMI: multimode interferometer; DBR: distributed Bragg reflector; PM: phase modulator; SOA: semiconductor optical amplifier.

input/output coupling loss). The 3 dB bandwidth and V_π of the push-pull MZM was ~ 10 GHz and 2.7 V, respectively. By tuning the phase difference of the RF signals for each MZM arm, up to 29 comb lines were obtained for an RF power of 26 or 27 dBm. In this case, the OFC had a comb spacing of 10 GHz and a flatness < 3 dB. By fine-tuning the phase difference, the odd or even 10 GHz tones could be suppressed; hence, a comb spacing of up to 20 GHz was achieved (here, there were 5 comb lines with a flatness < 3 dB).

In Ref. [44], Andriolli *et al.* reported an InP-based OFC generator which integrated a tunable distributed Bragg reflector laser diode (DBR-LD), an MZM, two PMs, and a semiconductor optical amplifier (SOA) on a chip occupying an area of 4.5×2.5 mm^2, see Fig. 4. The half-wave voltages V_π of the 1 mm long MZM and PMs were ~ 5 V. An OFC comprising 28 lines with a comb spacing of 4–5 GHz and a spectral flatness within 5 dB was obtained by driving the MZM and PMs with the RF signals at the same frequency. The on-chip losses were compensated using the SOA and the maximum output power was –4 dBm. While it was possible to increase the comb spacing to 10 GHz, the number of comb lines decreased to 11 because of the limited driving voltage of the RF signal.

To increase the number of comb lines, Bontempi *et al.* exploited a dual-drive configuration[45] for the MZM using the same integrated circuit design shown in Ref. [44]. Here, one arm of the MZM was driven with an RF signal at frequency f, while the other arm and the PMs were driven by a synchronous RF signal at frequency $3f$. They achieved an OFC with 44 comb lines, a comb spacing of 1 GHz, and a spectral flatness of 3 dB. By injecting multiple CW laser lines, they were able to wavelength multiplex multiple OFCs to increase the overall operating bandwidth. In particular, using an external multi-wavelength source, they generated and combined two OFCs centered at 1552 nm (~17 comb lines with ~3 dB flatness) and 1553 nm (~11 comb lines with ~3 dB flatness).

3.2. OFC generation in $LiNbO_3$

Lithium niobate is an excellent photonic material due to its advantages of large second order nonlinearity and ultrabroad transparent window from 350 to 5000 nm[59]. Recently, the rapid development of micro and nano fabrication techniques has allowed for the realization of high quality integrated optical devices based on LNOI, including low-loss and

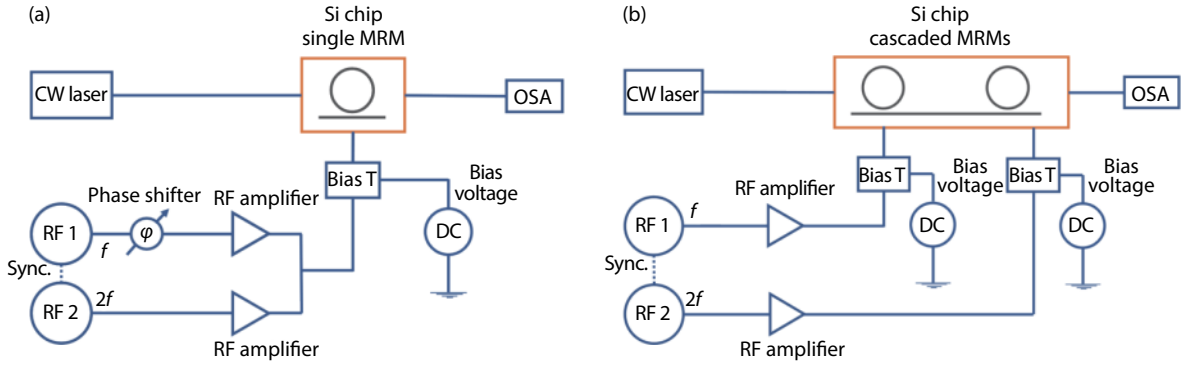

Fig. 5. (Color online) Typical experimental setup for OFC generation using (a) single MRM, (b) cascaded MRMs.

highly-confined optical waveguides[59, 60], high Q micro-resonators[60, 61], and EO modulators with very high bandwidth and low V_π[38, 62, 63]. As a result, LNOI is attracting considerable interest as an ideal platform for integrated EO OFC generation. Ren *et al.*[38] demonstrated an EO LNOI PM which can operate over a broad frequency range from 5 to 40 GHz and with V_π of 3.5 to 4.5 V and an on-chip loss as low as 1 dB. By driving this single PM with an RF signal corresponding to a phase shift of $4V_\pi$, an OFC comprising > 40 comb lines, a comb spacing of 30 GHz, and spanning the wavelength range from 1565 to 1575 nm was generated. Since a single PM is used, though, the comb exhibits the typical 'bat ears' and has a relatively large amplitude variation (for the central 30 comb lines, the flatness is within 10 dB). Another approach to broadening the comb bandwidth further is to use an EO modulator assisted with an optical resonator to increase the nonlinear EO interaction strength[20, 37, 41]. For example, in Ref. [41], a 4 mm long EO PM was incorporated within a Fabry-Pérot resonator formed by two distributed Bragg reflectors, each with a maximum reflectivity of ~ 98%. The resonator had a Q 4×10^5 and an FSR of 16.3 GHz and an insertion loss of 1.35 dB; the corresponding OFC had 18 comb lines; however, the comb spectrum is peaked at the carrier wavelength and the amplitude rolls of at a rate of ~ 18 dB/nm. As a second example, Zhang *et al.* also combined EO phase modulation with a microring resonator[20]. In this case, the microring had a loaded Q 1.5×10^6 and the modulation frequency was set near the FSR of the resonator. The microwave peak driving voltage is 10 V, corresponding to $1.2V_\pi$. An OFC spanning the wavelength range from 1560 to 1640 nm with more than 900 unique frequencies spaced by 10.453 GHz was obtained; while the comb spectrum is peaked at the carrier wavelength as in Ref. [41], the amplitude rolls of at ~1 dB/nm.

3.3. OFC generation in SOI

3.3.1. Microring modulators

Two setups commonly employed for OFC generation with MRMs are shown in Fig. 5. In Fig. 5(a), the output from two RF signal generators, one at f and the other at $2f$, is used to drive a single MRM (the phase difference between the two RF signal generators is tuned using a phase shifter). In Fig. 5(b), two cascaded MRMs are used, each driven by a separate RF signal generator. In both cases, the OFC spectrum depends on the operating conditions as described in Section 2.

In Ref. [34], a CMOS compatible process was used to fabricate an intracavity MRM. The microring had a radius of 14 μm and a coupling gap of 240 nm to the bus waveguide (for operation near the critical coupling point). The bus and ring waveguides had a width of 450 nm, a height of 220 nm, and a slab height of 90 nm. The waveguides were loaded with a PN junction implanted with phosphorus and boron to form N and P regions, respectively. For this design, a π phase shift could be obtained at critical coupling, which was achieved at a forward bias voltage of 1 V. An OFC with 5 comb lines, a comb spacing up to 10 GHz, and a flatness within 0.7 dB was obtained using a setup similar to that shown in Fig. 5(a).

In Ref. [47], an OFC comprising 12 comb lines with a comb spacing of 10 GHz was achieved using an MRM followed by a microring filter. The device was fabricated on a 220 nm SOI platform. A lateral PN junction was loaded on the circumference of the ring to deplete the free carriers. At zero bias voltage, the device had an extinction ratio of 20 dB (confirming operation near the critical coupling point). In reverse bias, the resonance exhibited a red-shift of ~ 27.5 pm/V. Both the MRM and microring filter were identical and designed with a radius of 7.5 μm and a coupling gap of 200 nm. The 3 dB bandwidth of the MRM was around 18 GHz. The microring filter was used to equalize the 5 middle lines.

In Ref. [48], Xu *et al.* proposed using cascaded MRMs for OFC generation using the frequency condition specified in Eq. (13). Both intracavity MRMs were identical, with a radius of 10 μm and a coupling gap of 315 nm. The lateral PN junctions covered 70% of the circumference, and the metal heater covered 95% of the circumference. The waveguides that form the microrings had a width of 500 nm, a height of 220 nm, and a slab height of 90 nm. When no bias voltage was applied, one MRM had an extinction ratio of 26 dB. The 3 dB bandwidth was measured to be about 25 GHz. Using a setup similar to that shown in Fig. 5(b) with RF signal generators at 20 and 10 GHz driving the first and second MRMs, respectively, they obtained an OFC with 5 comb lines, a comb spacing of 10 GHz, and a flatness within 8 dB.

We also investigated the use of cascaded MRMs for EO OFC generation[49, 50]. In contrast with Ref. [48], our MRMs are based on a microring coupled to a 2×16 μm^2 multimode interference (MMI) coupler; the waveguide that shapes the ring is loaded with a PN junction while the MMI coupler is loaded with a PIN junction. The MMI is added to increase the fabrication tolerance and to make the modulator less sensitive to polarization variations[64]. Phosphorus and Boron were used to create the N and and P regions, respectively. The bus and mi-

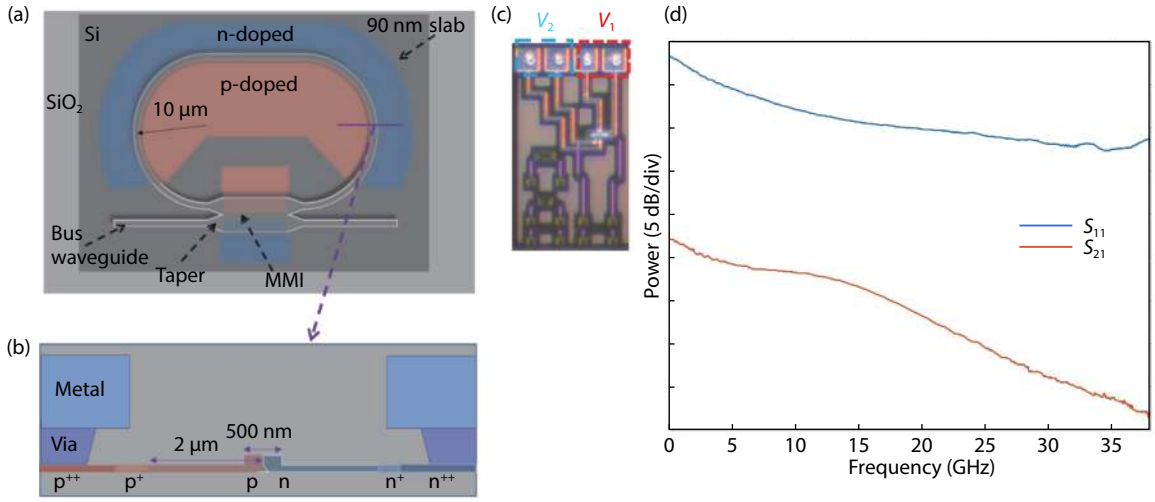

Fig. 6. (Color online) (a) Schematic of the proposed MRM. (b) Cross-section of the PN junction of the ring. (c) Microscopic image of one MRM. (d) S_{11} and S_{21} measurements of one MRM.

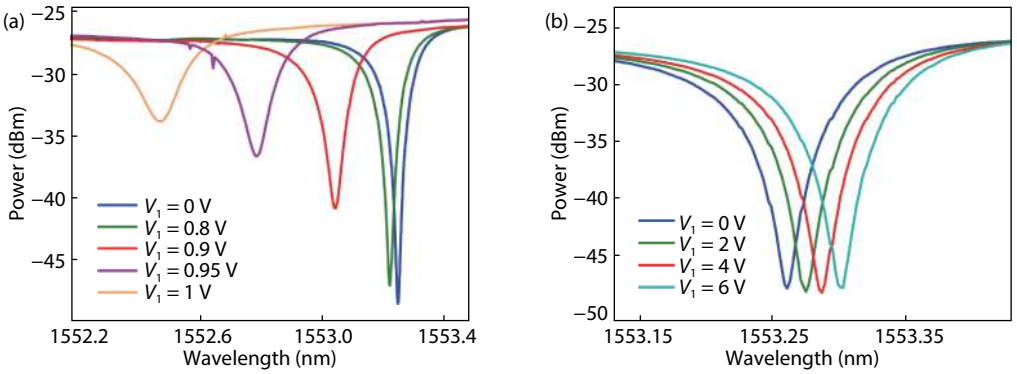

Fig. 7. (Color online) Transmission spectrum of one MRM in (a) forward bias and (b) reverse bias.

croring waveguides were 500 nm in width, 220 nm in height, and 90 nm in slab height. Two 14 μm linear tapers were added between the MMI section and the input-output waveguides to reduce the mode mismatch loss. Fig. 6 shows the schematic diagram of the MRM, the cross-section of the PN junction loaded on the microring, and a microscopic image of one MRM. A voltage of 1.6 V was required to obtain a π phase shift for each 1 cm of the rib waveguide.

For OFC generation, we only focused on driving the PN junction (microring waveguide) with no voltage applied to the MMI. We start by identifying the DC characteristics of one MRM by applying forward bias and reverse bias in the PN junction as shown in Figs. 7(a) and 7(b), respectively. When there is no voltage applied to the microring, the device exhibits a deep resonance at around 1553.3 nm. Under forward bias, there is a blue-shift in the resonant wavelength since free carriers are injected into the PN junction causing a reduction in the refractive index. The opposite phenomenon occurs under reverse bias (red-shift). Fig. 6(d) shows the measured S_{11} and S_{21} responses of a single MRM; the 3 dB bandwidth normalized to the value at 1.5 GHz is ~ 5 GHz.

Fig. 8(a) shows the experimental setup for OFC generation. We start by aligning the two ring's resonances on top of each other and operate the CW laser on the most linear region as discussed in Section 2. When we use the operating conditions given in Eq. (11), i.e., $f_1 = \frac{f_2}{3}$, we obtain 7 comb lines with comb spacing of 5 GHz (for a total bandwidth of 35 GHz) and an amplitude variation within 5 dB as illustrated in Fig. 8(c). If the operating condition is flipped, i.e., $f_2 = \frac{f_1}{3}$, the comb lines are no longer equidistant. When we use the frequency conditions of Eq. (13) ($f_1 = 2f_2$), we obtain 5 comb lines with frequency spacing of 5 GHz and amplitude variations within 4 dB, see Fig. 8(b). For this operating condition, we can also obtain a comb bandwidth of up to 50 GHz, as shown in Fig. 8(d). The temporal waveforms match with the simulated sinc-shaped Nyquist pulses (the ideal waveforms assume a perfect flat comb spectrum while the simulation waveforms are based on the measured amplitudes of the comb lines).

From the previous reported cases, the output frequency comb spectrum is limited by the 3 dB bandwidth of the MRM used. The comb amplitude variations are limited by the resonance steep (extinction ratio), namely, if the MRM operates in its critical coupling, the intensity at the resonance wavelength exhibit an abrupt π phase shift indicating a better modulation efficiency than over-coupling or under-coupling conditions. The number of comb lines depends on the frequency conditions used to drive the RF signal generators as discussed before.

3.3.2. Dual-drive MZMs

Recently Lin *et al.* explored the use of a single DD-MZM

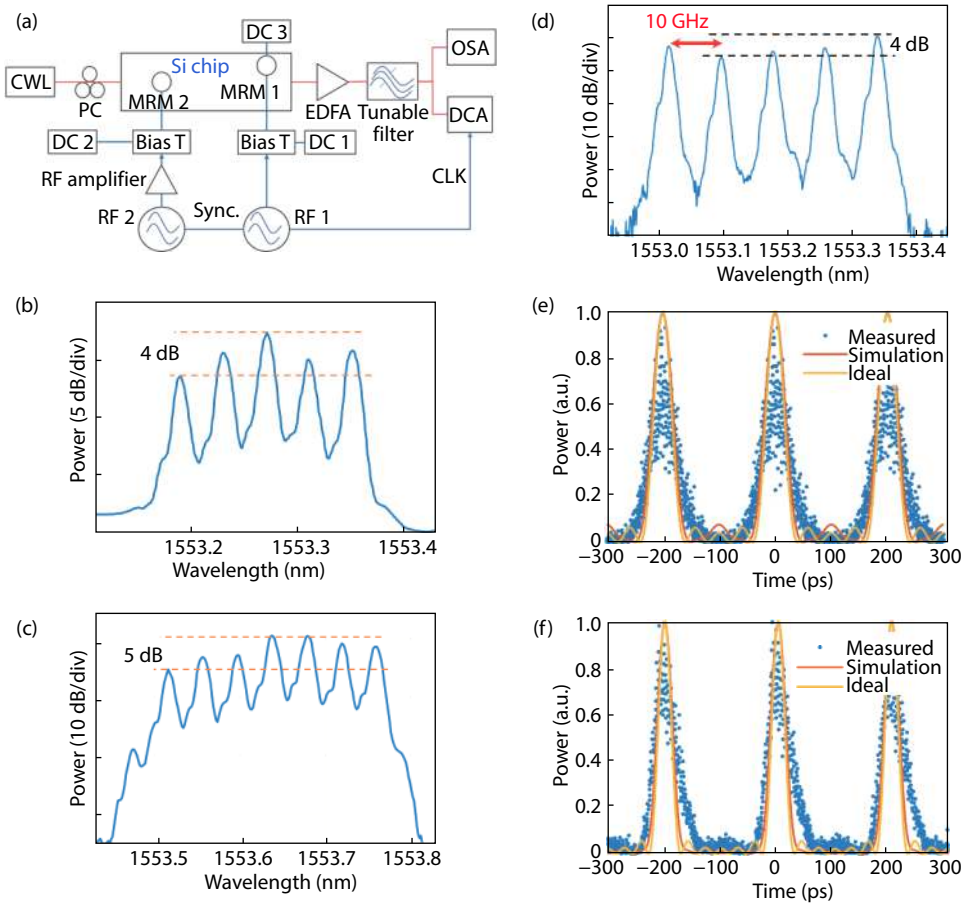

Fig. 8. (Color online) (a) Experimental setup. (b) Driving MRM 1 with 10 GHz and MRM 2 with 5 GHz. (c) Driving MRM 1 with 5 GHz and MRM 2 with 15 GHz. (d) Comb spectrum demonstrating 5 lines when driving MRM 1 at 20 GHz and MRM 2 at 10 GHz. (e) Temporal waveform of (b). (f) Temporal waveform of (c).

in SOI for EO OFC generation[17]. The modulator was based on depletion-mode PN junctions as phase shifters for high speed operation as well as heaters in the interferometer arms for fine-tuning the phase. Rib waveguides were used with a width of 500 nm, a height of 220 nm, and a slab height of 90 nm. The length of the phase shifters was 4.5 mm, and the half-wave voltage V_π is ~ 6 V. The modulator had a 3 dB bandwidth of 16.8 GHz at a reverse bias voltage of –3.5 V. For OFC generation, two RF signal generators at 20 and 40 GHz frequency were used to drive the upper and lower arms of the DD-MZM, respectively. 5 comb lines with a comb spacing of 20 GHz were obtained with spectral flatness within 9 dB, and a tone-to-noise ratio of 40 dB after amplification. To demonstrate the quality of the comb lines, each was used for Nyquist-WDM transmission and a bit rate up to 800 Gb/s was achieved with 16 Gbaud 32 QAM modulation; each channel had a BER below 2×10^{-2}.

3.3.3. Cascaded MZMs

Fig. 9 shows the principle of OFC generation using cascaded MZMs, which is a generalization of Fig. 3 and the operating conditions specified in Eq. (11). As the DC bias of each MZM has an impact on the power level of each comb line, we can shape the spectral profile of the OFC by tuning the DC bias for each MZM. One important application of this schematic is to generate sinc-shaped Nyquist pulses, or correspondingly, an OFC with a rectangular spectral profile. Note that while it is possible to generate OFCs by cascading several PMs, especially to increase the number of comb lines, this comes at the expense of degraded sideband suppression[52, 53].

Liu *et al.* demonstrated OFC generation using a cascaded MZM and PM[52] as well as cascaded MZMs[53]. The schematic and cross-section of the modulators are shown in Fig. 10. In these designs, both the MZM and PM were designed with TWEs and L-shaped PN junctions. In general, the slab height, rib height, and rib width of the rib waveguide are 90, 220, and 500 nm, respectively; the net doping concentrations are 4×10^{17} cm^{-3} for the p-type region and 8×10^{17} cm^{-3} for the n-type region. The lengths of the PN junctions in the MZM and PM are 3 mm. In the former configuration, 15 comb lines were obtained with comb spacing at 5 GHz with a flatness of 6 dB. In the latter configuration, each MZM as a bandwidth of ~13.5 GHz and V_π~ 3 V. An OFC with 9 comb lines, comb spacing of 5 GHz, and a flatness < 1.8 dB was obtained. When the operating parameters were adjusted to improve the suppression of higher-order sidebands, the temporal waveform corresponding to the OFC became more similar to an ideal sinc-shaped Nyquist pulse. In particular, the rms errors between the measured temporal waveforms and the ideal sinc-shaped Nyquist pulses were decreased from 0.0398 to 0.0368, when improving the suppression of the closest higher-order sideband to ~ 19 dB and of the next higher-order sideband to ~ 24 dB[53].

We have also demonstrated OFC and Nyquist pulse generation using two cascaded MZMs[51]. Our configuration com-

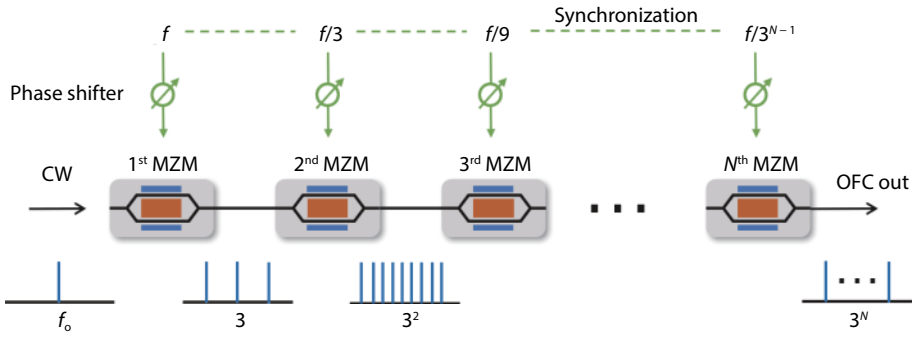

Fig. 9. (Color online) Schematic of cascaded MZMs for OFC generation.

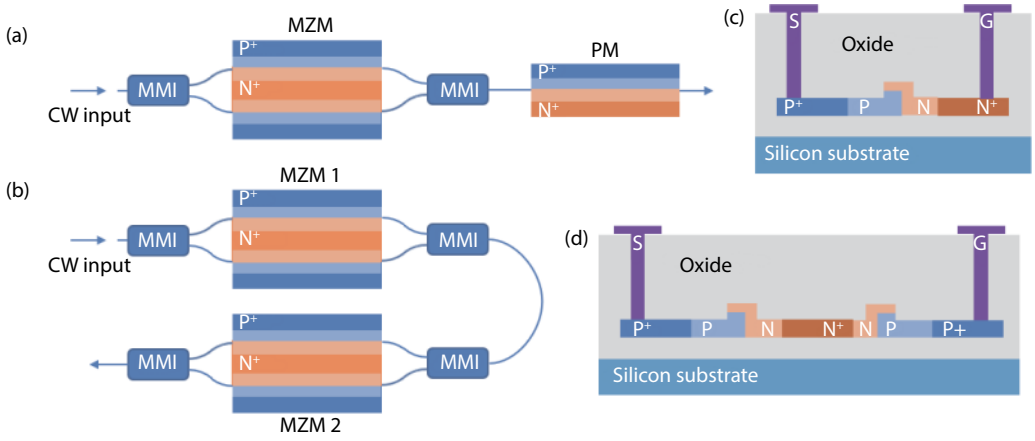

Fig. 10. (Color online) Schematic of integrated cascaded MZM and PM (after Ref. [48]) and cascaded MZMs for EO OFC (after Ref. [53]).

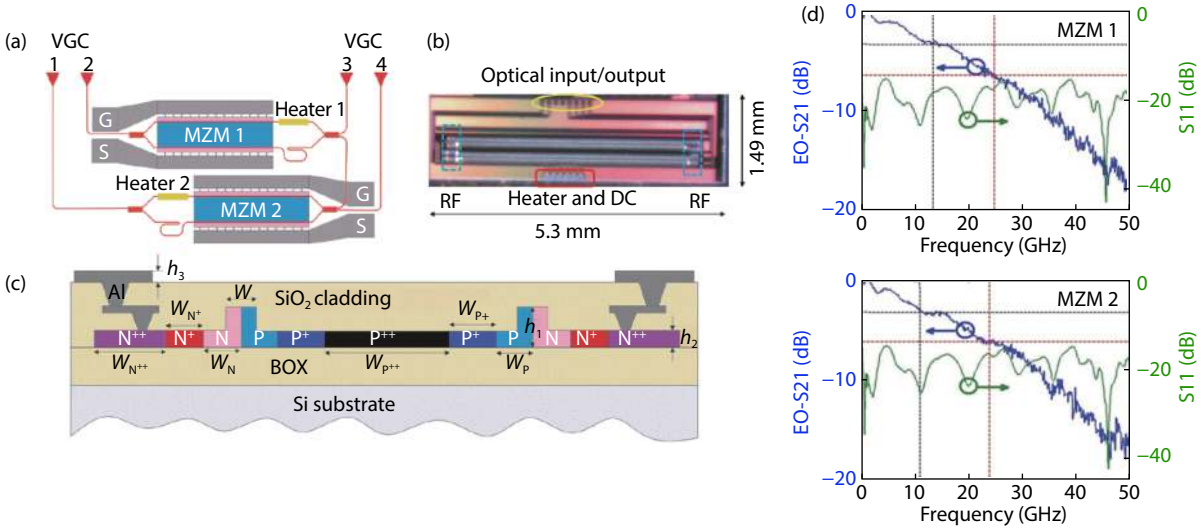

Fig. 11. (Color online) Schematic of the OFC generator in silicon photonics.

Table 1. Parameters of the TW-MZM[51].

Parameter	Value	Parameter	Value
h_1	220 nm	W_{N+}	0.81 μm
h_2	90 nm	W_N	0.39 μm
h_3	2 μm	W_{P++}	28 μm
W	500 nm	W_{P+}	0.83 μm
W_{N++}	5.2 μm	W_P	0.37 μm

prises two cascaded travelling wave MZMs (TW-MZMs) with 3 dB bandwidths ~ 12 GHz, as shown in Fig. 11. Four vertical grating couplers (VGCs) were designed for optical in/out. In particular, VGC 1 (output) and VGC 2 (input) were used for OFC generation while VGC 3 and VGC 4 were designed for characterization of MZM 1 and MZM 2 by coupling CW light into VGC 2 and VGC 1, respectively. For the TW-MZMs, the rib waveguide has the same configuration with the design in Refs. [48, 49], while the lateral PN junctions are used for the phase shifts. The TW-MZM design and parameters are shown in Fig. 11(c) are specified in Table 1. The TW-MZM uses a push-pull configuration and has a path imbalance of 130 μm

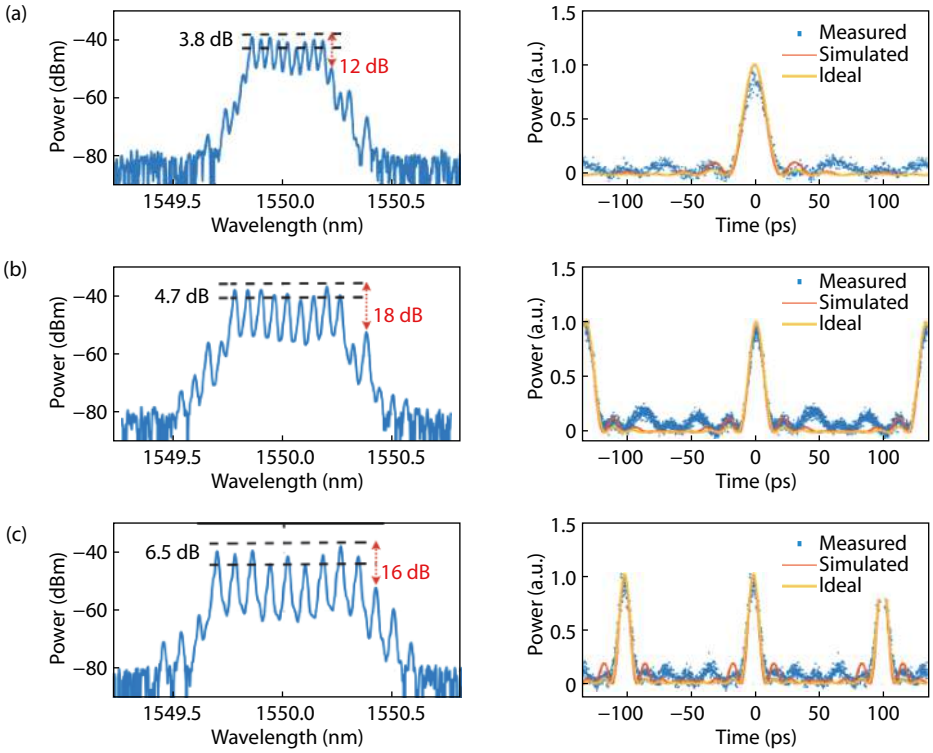

Fig. 12. (Color online) Experimental results of the OFC in silicon photonics. (a–c) the OFCs with spacing from 5, 7.5, and 10 GHz; left: spectral profile; right: temporal signals.

and a length ~ 4.55 mm (the net PN junction length is 4.2 mm). An n^{++} doped heater is located at the upper arm for tuning the phase. The half-wave voltages V_π of both MZMs are 10 V and the π phase shift can also be obtained at a heating voltage of 2.5 V.

For OFC generation, the CW light was injected into VGC 2 and a quasi-flat OFC can be obtained from VGC 1 by manipulating the heating voltages and reverse DC bias. Compared with the previous results in Ref. [53], we extended the comb spacing to 10 GHz (for an overall bandwidth up 90 GHz) with improved spectral flatness (see Fig. 12). In our experiments, we obtained comb spacings of 5, 7.5, and 10 GHz; the corresponding spectral flatness is 3.8, 4.7, and 6.5 dB, see Fig. 12. The flatness of the quasi-rectangular OFC degrades when the comb spacing is increased; higher RF power and the heater voltages need to be further optimized to improve the flatness. The corresponding temporal waveforms are shown in Fig. 12 and are in great agreement with ideal sinc-shaped Nyquist pulses (assuming a perfect rectangular OFC shape). The full width half maximums for the waveforms in Figs. 10(a), 10(b), and 10(c) are 17.6, 13.1, and 11.4 ps; the corresponding rms timing jitters are 1.2, 1.7, and 1.1 ps, respectively, showing the high quality of the generated pulses.

4. Outlook

Integrated technologies for EO OFC generation have been attracting growing attention in recent years. A summary of results obtained using InP, LNOI, and SOI is given in Table 2.

One of the greatest advantages of using InP is the integration of optical sources with modulators, as well as optical amplifiers to increase the output power. Although only modest output powers (e.g., –4 dBm) have been reported to date, higher values should be possible, e.g., using booster SOA designs. Moreover, wavelength multiplexing of locked integrated multi-wavelength sources is possible thereby allowing for the generation of broadband combs for various applications such as Nyquist WDM transmission[16].

With SOI, while the number of comb lines demonstrated to date has been modest, the spectral flatness has been reasonable, corresponding to the generation of Nyquist pulses of high quality. Moreover, the comb spacing achieved is comparable to commercial $LiNbO_3$ waveguide modulators. Silicon photonic modulators with bandwidths up to 45 GHz have been demonstrated[65]; however, careful circuit design is essential to limit parasitics that can otherwise reduce bandwidth in cascaded configurations. One of the main advantages of SOI is that a wide range of high performance passive devices, such as optical filters and dispersive delay lines, are readily available, allowing for the design of integrated subsystems capable of realizing complex functions with high performance. For example, combining cascaded modulators that allow for tunable OFC generation with programmable multi-functional integrated nanophotonics[66] opens the door for numerous optical and MWP signal processing applications. On the other hand, the fiber-to-fiber loss will still need to be addressed. While improved VGC designs can reduce coupling loss, the lack of on-chip amplification compared to InP can limit the amount of processing that can be performed, e.g., even when using high performance programmable devices as the typical silicon nanowire waveguide propagation loss is on the order of 1.5 to 3 dB/cm. In this context, hybrid integration with InP should be considered or may be required.

Perhaps the most exciting development has been the realization of efficient EO phase shifters and modulators in LNOI. PMs with resonators can certainly achieve a very large num-

Table 2. Summary of integrated EO OFC generation results.

Reference	Schematic	Number of comb lines	Comb spacing (GHz)	Flatness(dB)	V_π(V)	$V_\pi \cdot L$ (V·cm)	Insertion loss (dB)
			InP				
[42]	Single MZM	9	12.5	<0.77	2.3	N/A	N/A
[43]	On-chip laser, MZM	29/5	10/20	<3	2.7	N/A	6
[44]	On-chip laser, MZM + 2 PMs	28/11	5/10	<5/10	5	0.5	N/A
[45]	Same as Ref. [44]	44/17	1/3	<3	5	0.5	N/A
			LNOI				
[38]	Single PM	>40	30	~ 10 dB for the central 30 comb lines	4.5	9	<1
[41]	PM with FP resonator	18	16.3	amplitude roll off of 18 dB/nm	N/A	N/A	1.4
[20]	PM with microring resonator	>900	10.453	amplitude roll off of 1 dB/nm	8.3	5.1	N/A
			SOI				
[34]	Single MRM	5	10	~ 0.7	1	N/A	5.5
[47]	MRM + microring filter	12	10	<0.86	N/A	N/A	N/A
[48]	Cascaded MRM	5	10	~ 8	N/A	N/A	13
[50]	Cascaded MRM	5	10	~ 4	N/A	1.6	26
[17]	DD-MZM	5	20	~ 9	6	2.7	N/A
[52]	MZM + PM	15	5	<6	3	0.9	N/A
[53]	Cascaded MZM	9	5	<1.8	3	0.9	20
[51]	Cascaded MZM	9	5/7.5/10	<3.8/4.7/6.5	10	4.2	24

ber of comb lines albeit with a sloped amplitude response (i.e., limited spectral flatness). They have low insertion loss and are compact. It should also be possible to realize cascaded modulators thereby allowing for the generation of broadband OFCs with reasonable spectral flatness. Such OFCs can be used for Nyquist OTDM or Nyquist WDM transmission. They can also be combined with various passive devices, including microring resonators or Bragg grating devices[67, 68] to realize integrated MWP subsystems as well as programmable multi-functional integrated nanophotonics on LNOI.

Acknowledgements

This research was supported in part by the Natural Sciences and Engineering Research Council of Canada and the Fonds du Québec – Nature et Technologies. We thank M. Ma, R. Adams, K. Yim, X. Jin, R. Maram, B. Naghdi, A. Sarmani, M. Jacques, and D. V. Plant for their contributions.

References

[1] Ye J, Cundiff S T. Femtosecond optical frequency comb: Principle, operation, and applications. Boston: Kluwer Academic Publishers, 2005

[2] Hargrove L E, Fork R L, Pollack M A. Locking of He–Ne laser modes induced by synchronous intracavity modulation. Appl Phys Lett, 1964, 5, 4

[3] Hänsch T W. Nobel lecture: Passion for precision. Rev Mod Phys, 2006, 78, 1297

[4] Hall J L. Nobel lecture: Defining and measuring optical frequencies. Rev Mod Phys, 2006, 78, 1279

[5] Udem T, Holzwarth R, Hänsch T W. Optical frequency metrology. Nature, 2002, 416, 233

[6] Suh M G, Yang Q F, Yang K Y, et al. Microresonator soliton dual-comb spectroscopy. Science, 2016, 354, 600

[7] Dutt A, Joshi C, Ji X C, et al. On-chip dual-comb source for spectroscopy. Sci Adv, 2018, 4, e1701858

[8] Suh M G, Vahala K J. Soliton microcomb range measurement. Science, 2018, 359, 884

[9] Wilken T, Curto G L, Probst R A, et al. A spectrograph for exoplanet observations calibrated at the centimetre-per-second level. Nature, 2012, 485, 611

[10] Steinmetz T, Wilken T, Araujo-Hauck C, et al. Laser frequency combs for astronomical observations. Science, 2008, 321, 1335

[11] Spencer D T, Drake T, Briles T C, et al. An optical-frequency synthesizer using integrated photonics. Nature, 2018, 557, 81

[12] Liang W, Eliyahu D, Ilchenko V S, et al. High spectral purity Kerr frequency comb radio frequency photonic oscillator. Nat Commun, 2015, 6, 7957

[13] Xu X Y, Wu J Y, Nguyen T G, et al. Advanced RF and microwave functions based on an integrated optical frequency comb source. Opt Express, 2018, 26, 2569

[14] Torres-Company V, Weiner A M. Optical frequency comb technology for ultra-broadband radio-frequency photonics. Laser Photonics Rev, 2014, 8, 368

[15] Imran M, Anandarajah P M, Kaszubowska-Anandarajah A, et al. A survey of optical carrier generation techniques for terabit capacity elastic optical networks. IEEE Commun Surv Tutorials, 2018, 20, 211

[16] Willner A E, Fallahpour A, Zou K H, et al. Optical signal processing aided by optical frequency combs. IEEE J Sel Top Quantum Electron, 2021, 27, 1

[17] Lin J C, Sepehrian H, Xu Y L, et al. Frequency comb generation using a CMOS compatible SiP DD-MZM for flexible networks. IEEE Photonics Technol Lett, 2018, 30, 1495

[18] Jones D J, Diddams S A, Ranka J K, et al. Carrier-envelope phase control of femtosecond mode-locked lasers and direct optical frequency synthesis. Science, 2000, 288, 635

[19] Ortigosa-Blanch A, Mora J, Capmany J, et al. Tunable radio-frequency photonic filter based on an actively mode-locked fiber laser. Opt Lett, 2006, 31, 709

[20] Zhang M, Buscaino B, Wang C, et al. Broadband electro-optic frequency comb generation in a lithium niobate microring resonator. Nature, 2019, 568, 373

[21] Stern B, Ji X C, Okawachi Y, et al. Battery-operated integrated frequency comb generator. Nature, 2018, 562, 401
[22] Kippenberg T J, Holzwarth R, Diddams S A. Microresonator-based optical frequency combs. Science, 2011, 332, 555
[23] Levy J S, Gondarenko A, Foster M A, et al. CMOS-compatible multiple-wavelength oscillator for on-chip optical interconnects. Nat Photonics, 2010, 4, 37
[24] Griffith A G, Lau R K W, Cardenas J, et al. Silicon-chip mid-infrared frequency comb generation. Nat Commun, 2015, 6, 1
[25] Kippenberg T J, Gaeta A L, Lipson M, et al. Dissipative Kerr solitons in optical microresonators. Science, 2018, 361, eaan8083
[26] Yi X, Yang Q F, Yang K Y, et al. Soliton frequency comb at microwave rates in a high-Q silica microresonator. Optica, 2015, 2, 1078
[27] Chen H J, Ji Q X, Wang H, et al. Chaos-assisted two-octave-spanning microcombs. Nat Commun, 2020, 11, 2336
[28] Parriaux A, Hammani K, Millot G. Electro-optic frequency combs. Adv Opt Photon, 2020, 12, 223
[29] Gheorma I L, Gopalakrishnan G K. Flat frequency comb generation with an integrated dual-parallel modulator. IEEE Photonics Technol Lett, 2007, 19, 1011
[30] Jiang Z, Huang C B, Leaird D E, et al. Optical arbitrary waveform processing of more than 100 spectral comb lines. Nat Photonics, 2007, 1, 463
[31] Wu R, Supradeepa V R, Long C M, et al. Generation of very flat optical frequency combs from continuous-wave lasers using cascaded intensity and phase modulators driven by tailored radio frequency waveforms. Opt Lett, 2010, 35, 3234
[32] Soto M A, Alem M, Amin Shoaie M, et al. Optical sinc-shaped Nyquist pulses of exceptional quality. Nat Commun, 2013, 4, 2898
[33] Weimann C, Schindler P C, Palmer R, et al. Silicon-organic hybrid (SOH) frequency comb sources for terabit/s data transmission. Opt Express, 2014, 22, 3629
[34] Demirtzioglou I, Lacava C, Bottrill K R H, et al. Frequency comb generation in a silicon ring resonator modulator. Opt Express, 2018, 26, 790
[35] Buscaino B, Zhang M, Lončar M, et al. Design of efficient resonator-enhanced electro-optic frequency comb generators. J Lightwave Technol, 2020, 38, 1400
[36] Cordette S, Vedadi A, Shoaie M A, et al. Bandwidth and repetition rate programmable Nyquist sinc-shaped pulse train source based on intensity modulators and four-wave mixing. Opt Lett, 2014, 39, 6668
[37] Yu M J, Wang C, Zhang M, et al. Chip-based lithium-niobate frequency combs. IEEE Photonics Technol Lett, 2019, 31, 1894
[38] Ren T H, Zhang M, Wang C, et al. An integrated low-voltage broadband lithium niobate phase modulator. IEEE Photonics Technol Lett, 2019, 31, 889
[39] Shams-Ansari A, Yu M J, Chen Z J, et al. Microring electro-optic frequency comb sources for dual-comb spectroscopy. CLEO: QELS_Fundamental Science, 2019, JTh5B. 8
[40] Zhang M, Reimer C, He L Y, et al. Microresonator frequency comb generation with simultaneous Kerr and electro-optic nonlinearities. Conference on Lasers and Electro-Optics, 2019
[41] Xu M Y, He M B, Liu X Y, et al. Integrated lithium niobate modulator and frequency comb generator based on fabry-perot resonators. Conference on Lasers and Electro-Optics, 2020
[42] Yokota N, Yasaka H. Operation strategy of InP Mach–Zehnder modulators for flat optical frequency comb generation. IEEE J Quantum Electron, 2016, 52, 1
[43] Slavík R, Farwell S G, Wale M J, et al. Compact optical comb generator using InP tunable laser and push-pull modulator. IEEE Photonics Technol Lett, 2015, 27, 217
[44] Andriolli N, Cassese T, Chiesa M, et al. Photonic integrated fully tunable comb generator cascading optical modulators. J Lightwave Technol, 2018, 36, 5685
[45] Bontempi F, Andriolli N, Scotti F, et al. Comb line multiplication in an InP integrated photonic circuit based on cascaded modulators. IEEE J Sel Top Quantum Electron, 2019, 25, 1
[46] Nagarjun K P, Jeyaselvan V, Selvaraja S K, et al. Generation of tunable, high repetition rate optical frequency combs using on-chip silicon modulators. Opt Express, 2018, 26, 10744
[47] Wu X R, Tsang H K. Flat-top frequency comb generation with silicon microring modulator and filter. Conference on Lasers and Electro-Optics, 2017
[48] Xu Y L, Lin J C, Dubé-Demers R, et al. Integrated flexible-grid WDM transmitter using an optical frequency comb in microring modulators. Opt Lett, 2018, 43, 1554
[49] Maram R, Naghdi B, Samani A, et al. Silicon microring modulator with a pin-diode-loaded multimode interferometer coupler. 2019 24th OptoElectronics and Communications Conference (OECC) and 2019 International Conference on Photonics in Switching and Computing (PSC), 2019
[50] Khalil M, Maram R, Naghdi B, et al. Electro-optic frequency comb generation using cascaded silicon microring modulators. OSA Advanced Photonics Congress (AP), 2020
[51] Wang Z F, Ma M, Sun H, et al. Optical frequency comb generation using CMOS compatible cascaded Mach–Zehnder modulators. IEEE J Quantum Electron, 2019, 55, 1
[52] Liu S Q, Wu K, Zhou L J, et al. Optical frequency comb generation and microwave synthesis with integrated cascaded silicon modulators. Conference on Lasers and Electro-Optics, 2018
[53] Liu S Q, Wu K, Zhou L J, et al. Optical frequency comb and nyquist pulse generation with integrated silicon modulators. IEEE J Sel Top Quantum Electron, 2020, 26, 1
[54] Dubé-Demers R, LaRochelle S, Shi W. Ultrafast pulse-amplitude modulation with a femtojoule silicon photonic modulator. Optica, 2016, 3, 622
[55] Marpaung D, Roeloffzen C, Heideman R, et al. Integrated microwave photonics. Laser Photonics Rev, 2013, 7, 506
[56] Ogiso Y, Ozaki J, Ueda Y, et al. Over 67 GHz bandwidth and 1.5 V $v\pi$ InP-based optical IQ modulator with n-i-p-n heterostructure. J Lightwave Technol, 2017, 35, 1450
[57] Williams K A, Bente E A J M, Heiss D, et al. InP photonic circuits using generic integration. Photon Res, 2015, 3, B60
[58] Kish F A, Welch D, Nagarajan R, et al. Current status of large-scale InP photonic integrated circuits. IEEE J Quantum Electron, 2011, 7, 1470
[59] Bazzan M, Sada C. Optical waveguides in lithium niobate: Recent developments and applications. Appl Phys Rev, 2015, 2, 040603
[60] Wu R B, Wang M, Xu J, et al. Long low-loss-litium niobate on insulator waveguides with sub-nanometer surface roughness. Nanomaterials, 2018, 8, 910
[61] Zhang M, Wang C, Cheng R, et al. Monolithic ultra-high-Q lithium niobate microring resonator. Optica, 2017, 4, 1536
[62] Wang C, Zhang M, Chen X, et al. Integrated lithium niobate electro-optic modulators operating at CMOS-compatible voltages. Nature, 2018, 562, 101
[63] He M B, Xu M Y, Ren Y X, et al. High-performance hybrid silicon and lithium niobate Mach–Zehnder modulators for 100 Gbit s^{-1} and beyond. Nat Photonics, 2019, 13, 359
[64] Xu D X, Densmore A, Waldron P, et al. High bandwidth SOI photonic wire ring resonators using MMI couplers. Opt Express, 2007, 15, 3149
[65] Jacques M, Xing Z P, Samani A, et al. 240 gbit/s silicon photonic Mach-Zehnder modulator enabled by two 2.3-Vpp drivers. J Light-

wave Technol, 2020, 38, 2877

[66] Pérez D, Gasulla I, Capmany J. Programmable multifunctional integrated nanophotonics. Nanophotonics, 2018, 7, 1351

[67] Baghban M A, Schollhammer J, Errando-Herranz C, et al. Bragg gratings in thin-film $LiNbO_3$ waveguides. Opt Express, 2017, 25, 32323

[68] Pohl D, Kaufmann F, Escalé M R, et al. Tunable bragg grating filters and resonators in lithium niobate-on-insulator waveguides. Conference on Lasers and Electro-Optics, 2020

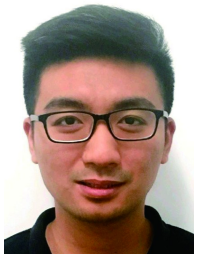

Hao Sun received the B.S. degree in physics from Shandong University in 2015 and the M.Eng. degree from the Institute of Semiconductors, Chinese Academy of Sciences, Beijing, China, in 2018. He is currently pursuing the Ph.D. degree in electrical and computer engineering with McGill University, Montreal, QC, Canada. His research interests include silicon photonics, optical communications, and microwave photonics.

Lawrence R. Chen has been with the Department of Electrical and Computer Engineering at McGill University since 2000. His research interests include optical communications, silicon photonics, and microwave photonics, as well as engineering education and teaching pedagogy.